PHILOSOPHICAL TRANSACTIONS A

rsta.royalsocietypublishing.org

Research

Article submitted to journal

Subject Areas:
Biomathematics, Differential Equations

Keywords:
Neural networks, synchronization, time delay, geometric singular perturbation

Author for correspondence:
Hwayeon Ryu
e-mail: hryu@hartford.edu

Geometric Analysis of Synchronization in Neuronal Networks with Global Inhibition and Coupling Delays

Hwayeon Ryu[1], and Sue Ann Campbell[2]

[1] Department of Mathematics, University of Hartford, West Hartford, CT 06117, USA

[2] Department of Applied Mathematics and Centre for Theoretical Neuroscience, University of Waterloo, Waterloo, Ontario, N2L 3G1, Canada

We study synaptically coupled neuronal networks to identify the role of coupling delays in network synchronized behavior. We consider a network of excitable, relaxation oscillator neurons where two distinct populations, one excitatory and one inhibitory are coupled with time-delayed synapses. The excitatory population is uncoupled, while the inhibitory population is tightly coupled without time delay. A geometric singular perturbation analysis yields existence and stability conditions for periodic solutions where the excitatory cells are synchronized and different phase relationships between the excitatory and inhibitory populations can occur, along with formulas for the periods of such solutions. In particular, we show that if there are no delays in the coupling oscillations where the excitatory population is synchronized cannot occur. Numerical simulations are conducted to supplement and validate the analytical results. The analysis helps to explain how coupling delays in either excitatory or inhibitory synapses contribute to producing synchronized rhythms.

THE ROYAL SOCIETY PUBLISHING

1. Introduction

Oscillatory behavior in neuronal networks has been one of the main subjects of study to better understand the central nervous system [6,30,37,57,66]. Examples of dynamic behaviors include synchronization [28,40], in which each cell in the network fires at the same time, and clustering [27,49], in which the entire population of cells breaks up into subpopulations or clusters; cells within a single population fire at the same time but are desynchronized from ones in different subpopulations. Much more complicated network behaviors [33,63,66], such as traveling waves [16,29,32,47,61], are also possible.

Neurons are connected mainly via chemical synapses, the junction of two nerve cells, through which information from one neuron transmits to another neurons, resulting in synaptic coupling. For this communication, the electrical signal must travel along the axon of one neuron to the synapse, resulting in a *conduction delay*. The size of this delay depends on the diameter and length of the axon and whether or not it is myelinated [65]. Further, once the electrical signal reaches the synapse, time is required for a neurotransmitter to be released and to travel through the synaptic cleft, a tiny gap between the nerve cells, and for the transmitter to cause an effect (through chemical reactions) on the postsynaptic cell. This time is called a *synaptic delay*. We call the combined effect of these two delays *coupling delay*. Synapses can be broadly classified into two types, excitatory and inhibitory, each associated with particular neurons. Excitatory synapses tend to promote the transmission of electrical signals while inhibitory synapses tend to suppress the transmission. Although excitatory neurons are much more common in the brain [20], it has become increasingly apparent that inhibitory neurons play an important role in producing and regulating the behavior of brain networks [48]. Thus it is important to consider networks including both inhibitory and excitatory neurons.

The synaptic types, length of the delays, network connectivity and intrinsic properties of the neurons all interact to produce a variety of dynamic network behaviors, such as synchronization and clustering [5,7,10,15,27,31,40,42,45,52,58,59]. Due to the richness of qualitatively different network behaviors caused by delays, the impacts of delays on such emergent network patterns are key to understanding the information processing functions in the brain. Many studies have been done on the effects of delays on networks where the synapses are exclusively excitatory or inhibitory [7,8,14,24,52], but few address networks with both [4,35,58,59]. Thus we focus on this case. There are many potential choices of network connectivity. We focus on a network with *global inhibition*, which consists of a uncoupled or sparsely coupled excitatory network reciprocally coupled to a highly connected inhibitory population. Networks with such structure are associated with rhythm generation in the CA1 region of hippocampus [3] and the thalamus [13,16,18], and with sensory processing [19,46]. In many of these networks, evidence exists that the inhibitory population is electrically coupled [2,12,26,36].

For the neural model, we focus on excitable, relaxation oscillators, the behavior of which is representative of many types of neurons. Thus our uncoupled neurons are not oscillatory, however, our network may exhibit oscillatory solutions and we prove sufficient conditions for the existence and stability of such solutions in terms of the coupling delays. These results help to provide insight into how the intrinsic properties of individual cells interact with the synaptic properties, including coupling type and delays, to produce the emergent population rhythms. For example, we show that the presence of coupling delays is necessary for our network to produce stable oscillatory behavior with the excitable cells synchronized.

We use geometric singular perturbation methods to analyze the mechanisms responsible for the emergence of network oscillations. The fundamental idea of this approach is to construct singular solutions by separating a system of differential equations into subsystems evolving on fast and slow time scales. Under some general hypotheses, actual solutions exist near these singular solutions. In the relaxation oscillator, the variables vary repeatedly between two distinct states corresponding to so-called *active* and *silent* phases. The amount of time spent in each phase substantially exceeds the time spent in the transitions between phases. When a relaxation

oscillator is used to model a neuron, the rapid transition from the silent phase to the active phase corresponds *firing* of an action potential in the neuron.

Geometric singular perturbation approaches have been previously used to investigate the generation of pattern formation in neuronal networks [4,8,9,24,34,35,38,55,56,62–64]. Many of these studies simplify their models to make mathematical analysis more tractable. The resulting simplified models lack key features: i) the direct interaction of coupling delays with intrinsic dynamics of neurons and ii) the underlying architecture of the network. For example, the effect of delay was considered in [8] but only for two neurons (i.e., not a network), and in [24,34] but for networks with a single type of neuron.

Networks of relaxation oscillators involving both excitatory and inhibitory neurons have been considered in several contexts. Motivated by bursting oscillations in the thalamus, [49–51] considered a global inhibitory network where both the excitatory and inhibitory cells are excitable, that is, in the absence of coupling neither cell type oscillates. They analyzed the existence and stability of synchronous solutions [51] and of clustered solutions [49]. However, their models have no conduction delay and the synaptic delay due to the chemical kinetics of the ion channel is implicitly included in the model for synaptic gating variable.

Several studies consider the effect of time delays in inhibition on oscillation patterns in networks of excitatory and inhibitory neurons. Motivated by networks of excitatory and inhibitory cells where there is presynaptic inhibition of the excitatory input to the inhibitory cells, Kunec and Bose [34] considered inhibitory networks with self inhibition. The unconnected inhibitory cells are nonoscillatory, with cells in a high voltage state. The analysis focuses on two cell networks, and considers the effect of time delay in the inhibition. They show how short time delays lead to anti-phase oscillations (the two neurons are half a period out of phase) and while long time delays lead to synchronized oscillations. They also show that a high voltage nonoscillatory state can coexist with these oscillations. Motivated by oscillations in the hippocampus, the effect of synaptic depression and inhibitory time delay on synchronization and cluster formation in network of excitatory cells and inhibitory cells was studied in the case where both cell types [35] or only the excitatory cells [9] are inherently oscillatory.

Here we consider a model for a global inhibitory network, where both the excitatory and inhibitory cells are excitable. We include an explicit representation of delays in the model equations which allows for a systematic study of the role of delays in producing network induced oscillations. Motivated by the fact that many inhibitory networks in the brain have gap junctional coupling, we assume the inhibitory cells are synchronized and represent them with a single cell. Our work can be considered an extension of the work in [49–51] to include the effect of explicit time delays. Our work is complementary to that in [9,35] as we consider networks where both cell types are nonoscillatory. Our work is similar in approach to that in [34], with some important differences both in setup and results. We focus on two excitatory cells and one inhibitory cell, and allow time delays in both the inhibitory and excitatory synapses. We show that there is a critical value of the total delay (sum of the excitatory and inhibitory delay). Below the critical value, the network does not oscillate. Above the critical delay the network oscillates, with the phase difference between the two populations determined by the relative time delays in the synapses. This is in contrast to the results of [34] where there are always network oscillations and the size of the delay determines the phase difference between the different cells.

Two important questions arise in the geometric analysis. The first is associated with the existence of a singular oscillatory solution. We assume that an individual cell, without synaptic input, is unable to oscillate. Thus, the existence of network oscillatory behavior depends on whether the singular trajectory is able to “escape" from the silent phase when they are coupled. The increased cellular or network complexity enhances each cell’s opportunity to escape from the silent phase. The second question is concerned with the stability of the singular solution. To demonstrate the stability, we need to show that the slightly perturbed trajectories of different cells are eventually brought closer together as they evolve in phase space. We show that this compression depends on the underlying network architecture as well as nontrivial interactions

between the intrinsic and synaptic properties of the cells [62]. Our analysis shows, for example, how delays promote stable oscillatory behaviors due to their interaction with intrinsic properties of neurons.

The remainder of the paper is organized as follows. In Section 2, we present the models for individual relaxation oscillators and for the dynamic coupling between oscillators which will be used in our study. Also we describe the architecture of the global inhibitory network consisting of two distinct populations of oscillators; one population inhibits the other, which in turn excites the first population. Section 2 also introduces the basic terminology needed for singular perturbation analysis, including the notion of a singular solution. In Section 3, we present the statement and proof of existence and stability results under conditions on size of the synaptic time delays. Section 4 follows to supplement our analytical results by illustrating the synchronous solutions obtained by numerical simulations. Finally, we conclude with a discussion in Section 5.

2. The Models

We describe the model equations corresponding to individual, uncoupled cells. There are two types: one for inhibitory cells and one for excitatory cells. Then, we introduce the synaptic coupling between the cells, delays, and network architecture to be considered. Finally, based on the model equations corresponding to the network, we consider fast and slow subsystems, which will be used for singular geometric analysis in subsequent sections.

(a) Single cells

We model an individual cell of the networks as a relaxation oscillator, whose equations are given by

$$\dot{x} = f(x, y), \tag{2.1}$$

$$\dot{y} = \epsilon g(x, y), \tag{2.2}$$

where $\dot{} = \frac{d}{dt}$, $x \in \mathbb{R}$, and $y \in \mathbb{R}^n$. For simplicity, we consider $n = 1$ in our analysis (see [50] for an example with $n > 1$). Here we assume $0 < \epsilon \ll 1$ for singular geometric analysis so that x is a fast variable and y is a slow variable. Also, we assume that the x-nullcline, $f(x, y) = 0$, is a cubic function, with left, middle, right branches, and $f > 0$ ($f < 0$) above (below) the x-nullcline curve. In addition, the y-nullcline is assumed to be a monotone decreasing function that intersects $f = 0$ at a unique fixed point, and $g > 0$ ($g < 0$) below (above) the y-nullcline curve. See Figure 1.

Depending on the location of the fixed point along the x-nullcline, we have different situations. The two most commonly seen in neural systems are the following: (i) the system is *excitable* if the fixed point lies on the left branch of $f = 0$, as labeled P_e in Fig. 1; (ii) the system is *oscillatory* if the fixed point lies on the middle branch of $f = 0$, labeled P_o. For the excitable system, P_e is an asymptotically stable fixed point corresponding to a negative value of x, and no periodic solutions arise for all small ϵ. However, if a sufficient amount of input is applied to the excitable system, the solution can jump to the right branch of $f = 0$ and remain there for some time before returning to the fixed point P_e, in this case we say the neuron *fires* or generates an action potential. On the other hand, in the oscillatory system, Eqs. (2.1)–(2.2) yield a periodic solution for all sufficiently small ϵ, as shown in Fig. 1. A third possibility is that the fixed point lies on the right branch of $f = 0$, in which case it is asymptotically stable. This corresponds to a cell with strong enough input that it ceases to fire and remains at a rest at a positive voltage, typically called *depoloarization block*. Since the thalamic cells motivating our study are known to be excitable during the sleep state [18,57], we will focus on the excitable case in subsequent sections.

(b) Synaptic coupling and network architecture

We consider networks with the architecture as shown in Fig. 2, which are motivated by models for the thalamic sleep rhythms [17,28]. In this architecture, called a *globally inhibitory network*, two

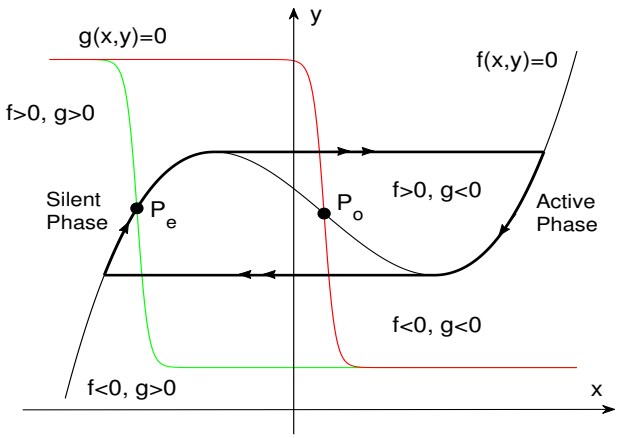

Figure 1. Nullclines for Eqs. (2.1)–(2.2) in both excitable (green line) and oscillatory (red line) cases. P_e and P_o correspond to the unique fixed points for excitable and oscillatory systems, respectively. The solid line shows a singular periodic solution for the oscillatory system. The double arrows on the solid lines indicate the fast jumps between the silent (left branch of the cubic curve) and active phases (right branch of the cubic curve). There are four different regions indicated depending on the signs of f and g.

distinct populations of cells interact with each other. Specifically, J-cells inhibit E-cells, which, in turn, excite the J population. However, there is no communication among E-cells. In the spindle rhythms, the cells within the J population are completely synchronized, thus we can view the entire J population as a single cell, sending inhibition to the E population globally. We assume that all E-cells are identical, but differ from the J-cell. To simplify the analysis, we shall assume that there are only two cells in the E population but this can be easily generalized to the case of an arbitrary number of E-cells.

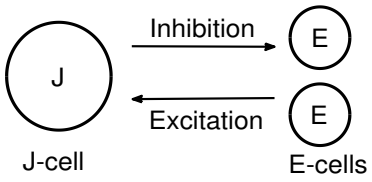

Figure 2. Schematic of the model with global inhibition. As the J-cells are synchronized, they are represented by one cell. The J-cell inhibits the E-cells, which, in turn, excite the J-cell.

The equations corresponding to each E_i for $i = 1, 2$ in the network are

$$\dot{x}_i = f(x_i, y_i) - g_{inh} s_J(x_J(t - \mathcal{T}_J))(x_i - x_{inh}), \tag{2.3}$$

$$\dot{y}_i = \epsilon g(x_i, y_i), \tag{2.4}$$

where f and g are defined as in Eqs. (2.1)–(2.2), and $g_{inh} > 0$ represents the maximal conductance of the synapse, which can be viewed as the coupling strength from the J-cell to each E-cell. The function s_J determines the *inhibitory* synaptic coupling from J to E. It is a sigmoidal function

which takes values in $[0,1]$. Since the J-cell sends inhibition to the E-cells, x_{inh}, the reversal potential for the synaptic connection, is set so that $x_i - x_{inh} > 0$. Finally, $\mathcal{T}_J$ denotes the delay in the inhibitory synapse.

The model equations for the J-cell are similarly given by

$$\dot{x}_J = f_J(x_J, y_J) - g_{exc}\left(\frac{1}{N}\sum_i s_i(x_i(t-\mathcal{T}_E))\right)(x_J - x_{exc}), \tag{2.5}$$

$$\dot{y}_J = \epsilon g_J(x_J, y_J), \tag{2.6}$$

where g_{exc} denotes the maximal conductance of the *excitatory* synapse from E to J. As in the model for the E-cell, the s_i are sigmoidal functions with values in $[0,1]$. The reversal potential for the *excitatory* synapse, denoted by x_{exc}, is chosen so that $x_J - x_{exc} < 0$. The delay in the excitatory synapse, τ_E, is assumed to be same for all the E-cells. For the case of two E-cells in the network, let us define $s_{tot} \equiv \frac{1}{2}(s_1 + s_2)$. Note that we do not incorporate chemical kinetics for synapses into our model. However, $\mathcal{T}_E$ and $\mathcal{T}_J$ include the effect of delays due to the chemical kinetics, as well as other factors.

Equations (2.3)–(2.6) form a four dimensional system of delay differential equations. The appropriate initial data for such a system specifies functions for the variables on the interval $-\mathcal{T} \leq t \leq 0$, where $\mathcal{T} = \max(\mathcal{T}_E, \mathcal{T}_J)$, yielding an infinite dimensional phase space. In our analysis, however, we will assume that the synaptic functions s_i and s_J are Heaviside step functions, thus the values switch between 0 and 1 at the threshold x-value. The system (2.3)–(2.6) then becomes a discontinuous or switched system of ordinary differential equations, with a delayed switching manifold. That is, at any time the system evolves according to the ODEs given by Eqs. (2.3)–(2.6) with the each of the s_i and s_J either 0 or 1, but the condition that determines which system of ODEs is followed depends on the delayed values of x_i and x_J. While there is a fairly large literature on the stability of such systems (see e.g., [25,60]), the bifurcation theory of such systems is still being developed, with many results to date based on direct analysis of specific systems [1,53,54], such as what we will carry out. In our numerical simulations we will take the synaptic functions to be smooth approximations of Heaviside step functions.

Remark 2.1. *An excitable cell stays at its stable fixed point unless it receives some synaptic input. The effect of this input depends on the type of coupling. For example, since $x_i - x_{inh} > 0$, inhibitory coupling decreases $\dot{x}_i$, making it harder for the E-cells to fire. On the other hand, since $x_J - x_{exc} < 0$ excitatory coupling increases $\dot{x}_J$, making it easier for the J-cell to fire. The main goal of our work is to show that the presence of time delayed synaptic coupling can give rise solutions where both neurons fire periodically, that do not exist in the uncoupled system or in the coupled system with no time delays.*

The present model is similar to the model developed in [51] in that both describe the dynamics of synaptic connection between two distinct populations in a globally inhibitory network. However, in their model, there are additional differential equations for the synaptic gating variables, s_i and s_J. In these equations other slow variables are introduced which ensure the existence of oscillatory solution. Our model, on the other hand, has no differential equations for the synaptic variables, and the synaptic coupling is a direct function of the appropriate x variable. However, we include time delays in the connections, as in [8,24]. Our model is different from that of [8,24] as in their models the uncoupled neurons are oscillatory, instead of excitable.

To conduct singular perturbation analysis, we identify the *fast* and *slow subsystems* for each population's evolution by dissecting the full system of equations given in Eqs. (2.3)–(2.6). The slow subsystem determines the evolution of the y-variable of each cell on either the left branch (the silent phase) or the right branch (the active phase) of its cubic nullcline. The fast subsystem determines the evolution of the x-variable of each cell as it jumps between the branches of the nullcline.

The *slow subsystem* is derived by first introducing a slow time scale $\tilde{t} = \epsilon t$, and then setting $\epsilon = 0$. This leads to a reduced system of equations for the slow variables only, after solving for

each fast variable in terms of the slow ones. For brevity, we focus on the derivation for the E-cell. In terms of the slow time scale equations (2.3)–(2.4) become

$$\epsilon x_i' = f(x_i, y_i) - g_{inh} s_J(x_J(\tilde{t} - \epsilon\mathcal{T}_J))(x_i - x_{inh}), \tag{2.7}$$

$$y_i' = g(x_i, y_i), \tag{2.8}$$

where $' = \frac{d}{d\tilde{t}}$. From this we can see that the size of the time delay, $\mathcal{T}_J$, is important in determining the solution of the slow subsystem. If $\mathcal{T}_J = O(1)$ with respect to ϵ (or smaller) then when we set $\epsilon = 0$ the effect of the time delay disappears, that is, $x_J(\tilde{t} - \epsilon\mathcal{T}_J) \approx x_J(\tilde{t})$. However, if $\mathcal{T}_J = O(1/\epsilon)$ then this term will persist. We will focus on this case in our work. Let $x = \Phi_L(y, s)$ denote the left branch of the cubic $f(x, y) - g_{inh} s(x - x_{inh}) = 0$, and $G_L(y, s) \equiv g(\Phi_L(y, s), s)$. Then we have the following equations

$$x_i = \Phi_L(y_i, s_J), \tag{2.9}$$

$$y_i' = G_L(y_i, s_J), \tag{2.10}$$

$$s_J = s_J(x_J(\tilde{t} - \tau_J)), \tag{2.11}$$

where $\tau_J = \epsilon\mathcal{T}_J$. The system in Eqs. (2.9)–(2.11) determines the slow evolution of the E-cell on the left branch. The slow subsystems of the E-cell on the right branch and of the J-cell on either branch can be similarly derived.

The *fast subsystem* of a singularly perturbed ODE system is obtained by setting $\epsilon = 0$ in the original equations. However, we must account for the time delays in our model. The scaling we have chosen means that the delays are large compared with the amount of time spent in the fast subsystem. Thus even if at time t the J-cell is evolving according to the fast subsystem, $x_J(t - \mathcal{T}_J)$ is most likely (with increasing likelihood as $\epsilon \to 0$) evolving according to the slow subsystem, and is effectively unchanged during the evolution on the fast subsystem. We thus set $x_J(t - \mathcal{T}_J) = \bar{x}_J$ which represents the value of x_J a time $\mathcal{T}_J$ before the evolution on the fast subsystem began. Using this in equations (2.3)–(2.4) and setting $\epsilon = 0$ we obtain the model for the fast subsystem of the E-cell

$$\dot{x}_i = f(x_i, y_i) - g_{inh} s_J(\bar{x}_J)(x_i - x_{inh}), \tag{2.12}$$

$$\dot{y}_i = 0 \tag{2.13}$$

where $\dot{} = \frac{d}{dt}$. The model for the fast subsystem of the J-cell can be similarly derived.

In summary, the slow subsystem describes the evolution of a cell along the left or right branch of some "cubic" nullcline, which is determined by the total amount of synaptic input that the cell receives. A fast jump occurs when one of the cells reaches the left or right "knee" of its corresponding cubic or the amount of synaptic input changes. When this occurs, the cell may jump from the silent to the active phase or vice versa or between branches of the same phase corresponding to different levels of synaptic input. The fast subsystem describes the evolution of a cell during a jump. In the $\epsilon \to 0$ limit, we can construct a *singular solution* by connecting the solution to the slow subsystem with jumps between branches given by solutions to the fast subsystem. The analysis we provide in this study focuses on such singular solutions. For the extensions to small positive ϵ, refer the work in [11,41,43].

Remark 2.2. *We analyze the dynamics of the network by constructing singular solutions. If g_{inh} is not too large, then $f(x, y) - g_{inh} s_J(x - x_{inh}) = 0$ represents a cubic-shaped curve for each $s_J \in [0, 1]$. Let us denote this curve by $\mathcal{C}_{s_J}$; curves $\mathcal{C}_0$ and $\mathcal{C}_1$ are shown in Figure 3A. The trajectory for E_i lies on the left/right branches of one of these curves ($\mathcal{C}^L_{s_J}/\mathcal{C}^R_{s_J}$) during the silent/active phase, respectively. Fast jumps between different phases occur when an E_i reaches the right knee of its respective cubic or the effect of inhibition by the J-cell wears off. Similarly, J lies on the cubic curve determined by its total synaptic input s_{tot}, denoted by $\mathcal{J}_{s_{tot}}$, as shown in Fig. 3B. Note in Fig. 3A that the $s_J = 1$ nullcline ($\mathcal{C}_1$) lies above the $s_J = 0$ nullcline ($\mathcal{C}_0$), while in Fig. 3B, the $s_{tot} = 1$ nullcline ($\mathcal{J}_1$) lies below the $s_{tot} = 0$ nullcline ($\mathcal{J}_0$).*

These relations result from the fact that the E_i receive inhibition from J while J receives excitation from the E_i.

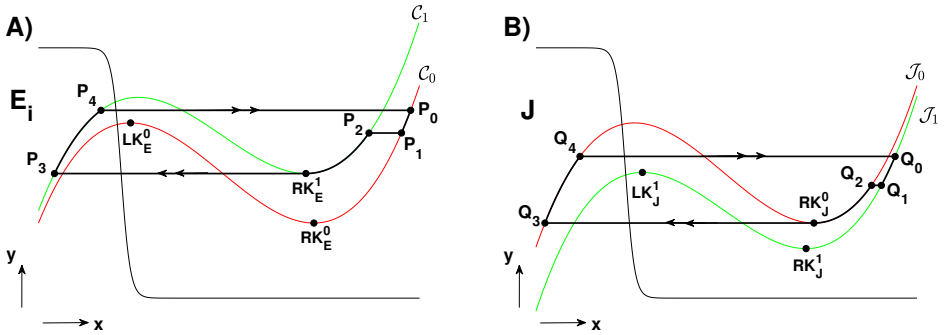

Figure 3. Plots of possible trajectories for A) E-cells and B) J-cell in black solid lines. The double arrows on the solid lines indicate the fast jumps between the silent and active phases. The trajectories shown are for the situation when there is a delay only in the inhibitory synapse. The points P_i and Q_i and the construction of this solution are discussed in section 3(a).

3. Model Analysis

In this section, we give sufficient conditions for the existence of a singular oscillatory periodic solution, and prove the stability of the solution in subsection (a). In subsection (b), we consider the case of no coupling delay and prove that oscillatory solutions with the E-cells synchronized do not exist.

In the following analysis, we denote the fixed point on $\mathcal{C}^L_{s_J}$ in Eqs. (2.3)–(2.4) by $FP^{s_J}_E = (x^F_E(s_J), y^F_E(s_J))$, the left knee by $LK^{s_J}_E = (x^L_E(s_J), y^L_E(s_J))$, and the right knee by $RK^{s_J}_E = (x^R_E(s_J), y^R_E(s_J))$. We similarly define the fixed point on $\mathcal{J}^L_{s_{tot}}$ in Eqs. (2.5)–(2.6) by $FP^{s_{tot}}_J = (x^F_J(s_{tot}), y^F_J(s_{tot}))$, the left knee by $LK^{s_{tot}}_J = (x^L_J(s_{tot}), y^L_J(s_{tot}))$, and the right knee by $RK^{s_{tot}}_J = (x^R_J(s_{tot}), y^R_J(s_{tot}))$. See Fig. 4.

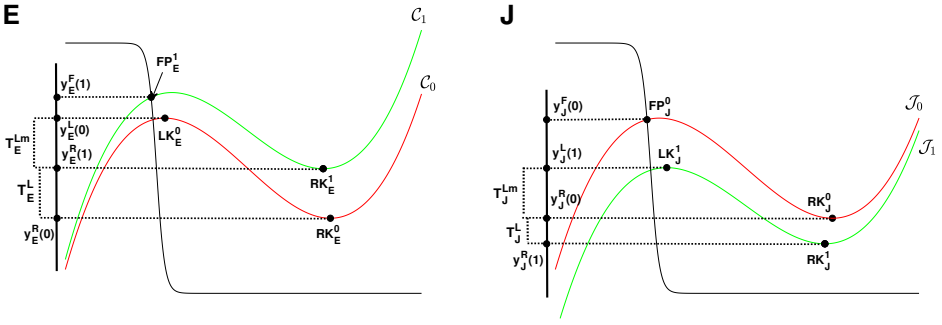

Figure 4. The two cubic nullclines corresponding to different levels of inhibitions for the E and J cells. The left and right knees and the equilibrium points used in the analysis are defined. The times of evolution between relevant points on the left branches of nullclines are also indicated. The times have been projected onto simplified versions of the branches. See Table 1 for details.

Let T_E^L be the travel time, in the slow subsystem, on $\mathcal{C}_1^L$ from $y_E^R(0)$ to $y_E^R(1)$ and T_E^{Lm} be the travel time on $\mathcal{C}_1^L$ from $y_E^R(1)$ to $y_E^L(0)$; see Fig. 4. Note that T_E^{Lm} and T_E^L are the same for $\mathcal{C}_0^L$. In a similar manner, we can define the analogous travel times for the the J-cell, T_J^L, T_J^{Lm}; see Fig. 4 and Table 1.

time	branch	start	end
T_E^L	$\mathcal{C}_1^L$	$y_E^R(0)$	$y_E^R(1)$
T_E^{Lm}	$\mathcal{C}_1^L$	$y_E^R(1)$	$y_E^L(0)$
T_J^L	$\mathcal{J}_0^L$	$y_J^R(1)$	$y_J^R(0)$
T_J^{Lm}	$\mathcal{J}_0^L$	$y_J^R(0)$	$y_J^L(1)$

Table 1. Travel times in the slow subsystem between relevant points on the nullclines of the E and J cells.

(a) Dynamics with delays

In this section, we prove the existence and stability for oscillatory periodic solutions when delays are present. Specifically, we give conditions with $\tau_J > 0$ and $\tau_E = 0$. All other possible cases follow from the results of [39].

Theorem 3.1. *A singular oscillatory periodic solution exists with non-zero τ_J and zero τ_E if*
(i) $y_E^F(1) > y_E^L(0)$ and $y_J^F(0) > y_J^L(1)$, and
(ii) the delay τ_J is sufficiently large, specifically $T_E^{Lm} + T_E^L + T_J^{Lm} + T_J^L < \tau_J$, where the values are defined in Table 1 and Fig. 4.

Remark 3.1. *As noted in the proof of [51], the condition $y_E^F(1) > y_E^L(0)$ indicates that the fixed point of $\mathcal{C}_1$ lies above the left knee of $\mathcal{C}_0$. This makes it possible for E-cells to fire (jump from the silent to the active phase) when they are released from inhibition. Similarly, the condition $y_J^F(0) > y_J^L(1)$ implies that the fixed point of $\mathcal{J}_0$ lies above the left knee of $\mathcal{J}_1$. This makes it possible for the J-cell to fire when the excitation from the E-cells turns on.*

Proof. We prove the existence of a singular oscillatory solution by constructing such a solution if the hypotheses of Theorem 3.1 are satisfied. The number of E-cells in the network is arbitrary. Since we are interested in solutions where the E-cells are synchronized, we assume the positions of the E-cells are identical throughout the construction. A possible singular trajectory is shown in Figure 3.

There are three possible cases for the trajectory of each cell. We first describe the situation for the E-cell, depending on its location in the active phase (along $\mathcal{C}_0^R$) when the inhibition due to the J-cell turns on, i.e., time τ_J after it jumps up.

Case 1: If the E-cell lies between the right knee of $\mathcal{C}_1$, RK_E^1, and the right knee of $\mathcal{C}_0$, RK_E^0, it jumps down to $\mathcal{C}_1^L$.

Case 2: If the E-cell lies above RK_E^1 it jumps to $\mathcal{C}_1^R$. It travels on $\mathcal{C}_1^R$ until it reaches RK_E^1 and jumps down to $\mathcal{C}_1^L$. This is visualized in Fig. 3A. Let T_E^* be the time spent on $\mathcal{C}_1^R$, i.e., from P_2 to RK_E^1 in Fig. 3A.

Case 3: If the E-cell reaches RK_E^0 before the inhibition due to the J-cell turns on, it jumps down to $\mathcal{C}_0^L$ and travels upwards along this branch until the inhibition turns on and it jumps to $\mathcal{C}_1^L$. Let $T_E^\dagger$ be the time spent on $\mathcal{C}_0^L$.

The description for the J-cell is similar, depending on its location in the active phase (along $\mathcal{J}_1^R$) when the excitation due to the E-cells turns off. This occurs as soon as they jump down because $\tau_E = 0$.

Case 1: If the J-cell lies between the right knee of $\mathcal{J}_0$, RK_J^0, and the right knee of $\mathcal{J}_1$, RK_J^1, it jumps down to $\mathcal{J}_0^L$. This is visualized in Fig. 5A.

Case 2: If the J-cell lies above RK_J^0 it jumps to $\mathcal{J}_0^R$. It travels on $\mathcal{J}_0^R$ until it reaches RK_J^0 and jumps down to $\mathcal{J}_0^L$. This is visualized in Fig. 3B. Let T_J^* be the time spent on $\mathcal{J}_0^R$, i.e., from Q_2 to RK_J^0 in Fig. 3B.

Case 3: If the J-cell reaches RK_J^1 before the excitation due to the E-cells turns off, it jumps down to $\mathcal{J}_1^L$ and travels upwards along this branch until the excitation turns off. This is visualized in Fig. 5B. Let $T_J^\dagger$ be the time spent on $\mathcal{J}_1^L$.

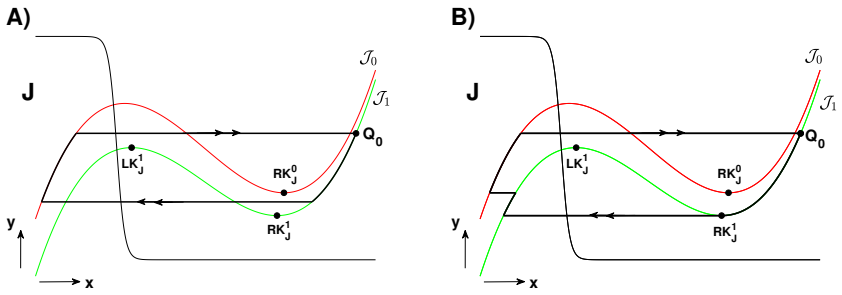

Figure 5. Plots of two different trajectories in x-y phase plane, depending on the position of the J-cell along $\mathcal{J}_1^R$ when excitation to the J-cell turns off.

We can put these together to find the active and silent phases of singular periodic solutions, if they exist. Let T_E^a, T_E^s be the length of the active and silent phases of the E-cell on the periodic orbit, and T_J^a, T_J^s similarly for the J-cell. The active phase includes time on the right branch of both the upper and lower nullclines. The silent phase includes time on the left branch of both the upper and lower nullclines. Then the period of the periodic orbit is $\mathcal{T} = T_E^a + T_E^s = T_J^a + T_J^s$.

Among all the possible cases, here we focus on one case, (E case, J case)$=(2,2)$, show the existence of its singular periodic trajectory, and derive the lower bound on τ_J in the hypothesis of Theorem.

We begin with the E-cells having just jumped up to $\mathcal{C}_0^R$, the point labeled P_0 in Fig. 3A. Due to the excitation from the E-cells and $\tau_E = 0$, the J-cell will immediately jump to $\mathcal{J}_1^R$, the point labeled Q_0 in Fig. 3B. Thus, the E-cells are still in the active phase when the J-cell jumps up. Since the E-cells are in Case 2, they lie above RK_E^1 after the τ_J delay. When inhibition turns on the E-cells jump from P_1 to P_2, as shown in Fig. 3A, while the J-cell evolves down along $\mathcal{J}_1^R$.

As the J-cell is in Case 2, it lies above RK_J^0 when the E-cells reach the right knee of $\mathcal{C}_1$, labeled RK_E^1 in Fig. 3A. Thus, at the time when E-cells jump down, labeled P_3 on $\mathcal{C}_1^L$, the J-cell jumps to the point Q_2 along $\mathcal{J}_0^R$ due to $\tau_E = 0$, as shown in Fig. 3B. Then, the J-cell moves down $\mathcal{J}_0^R$ while the E-cells move up $\mathcal{C}_1^L$. When the J-cell reaches the right knee RK_J^0, it jumps down to the point Q_3 on $\mathcal{J}_0^L$.

Now the inhibition to E-cells starts to turn off. However, due to the delay τ_J in inhibition, this means that the E-cells do not jump to $\mathcal{C}_0^L$ but continue to move up $\mathcal{C}_1^L$ instead. Moreover, if the inhibitory delay, τ_J, is sufficiently large, the E-cells are able to reach a point (P_4) above LK_E^0, and to jump up to P_0 on $\mathcal{C}_0^R$ again when they are finally released from inhibition. When the E-cells jump up, if τ_J is sufficiently large, the J-cell also lies above LK_J^1. Therefore, it also jumps to $\mathcal{J}_1^R$ and returns to its starting point, Q_0. In the following we will derive a lower bound on how large τ_J must be for these arguments to hold.

Recall that $y_E^L(s_J)$ (or $y_E^R(s_J)$) is the y-value of the left (or right) knee of $\mathcal{C}_{s_J}$ and we have $y_E^R(0) < y_E^L(0)$. From Fig. 4 T_E^{Lm} is the time for y to increase from $y_E^R(1)$ to $y_E^L(0)$ under $y' = G_L(y,1)$ in the slow subsystem. Thus, in the case we consider, (E, J)$=(2,2)$, we need T_E^{Lm} less

(E, J)	T_E^a	T_E^s	T_J^a	$\mathcal{T}$	τ_J lower bound
(1, 1)	τ_J	τ_J	τ_J	$2\tau_J$	$\max(T_E^{Lm}+T_E^L, T_J^{Lm}+T_J^L)$
(1, 2)	τ_J	$\tau_J+T_J^*$	$\tau_J+T_J^*$	$2\tau_J+T_J^*$	$\max(T_E^{Lm}+T_E^L, T_J^{Lm})$
(1, 3)	τ_J	$\tau_J-T_J^\dagger$	$\tau_J-T_J^\dagger$	$2\tau_J-T_J^\dagger$	$T_E^{Lm}+T_E^L+T_J^{Lm}+T_J^L$
(2, 1)	$\tau_J+T_E^*$	τ_J	$\tau_J+T_E^*$	$2\tau_J+T_E^*$	$\max(T_E^{Lm}, T_J^{Lm}+T_J^L)$
(2, 2)	$\tau_J+T_E^*$	$\tau_J+T_J^*$	$\tau_J+T_J^*+T_E^*$	$2\tau_J+T_J^*+T_E^*$	$\max(T_E^{Lm}, T_J^{Lm})$
(2, 3)	$\tau_J+T_E^*$	$\tau_J-T_J^\dagger$	$\tau_J-T_J^\dagger+T_E^*$	$2\tau_J-T_J^\dagger+T_E^*$	$T_E^{Lm}+T_J^{Lm}+T_J^L$
(3, 1)	$\tau_J-T_E^\dagger$	τ_J	$\tau_J-T_E^\dagger$	$2\tau_J-T_E^\dagger$	$\max(T_E^{Lm}+T_E^L, \tau_J^{Lm}+T_J^L)$
(3, 2)	$\tau_J-T_E^\dagger$	$\tau_J+T_J^*$	$\tau_J+T_J^*-T_E^\dagger$	$2\tau_J+T_J^*-T_E^\dagger$	$\max(T_E^{Lm}+T_E^L, T_J^{Lm})$
(3, 3)	$\tau_J-T_E^\dagger$	$\tau_J-T_J^\dagger$	$\tau_J-T_J^\dagger-T_E^\dagger$	$2\tau_J-T_J^\dagger-T_E^\dagger$	$T_E^{Lm}+T_E^L+T_J^{Lm}+T_J^L$

Table 2. Summary of the values of T_E^a, T_E^s, T_J^a, the period $\mathcal{T}$, and the lower bound on τ_J for existence in all nine cases.

than the duration of the E-cell silent phase, T_E^s, for the oscillatory solution to exist. Similarly for the J-cell to escape from the silent phase, we need T_J^{Lm} less than T_J^s.

The duration of J-cell active phase, T_J^a, consists of up to three different parts: (i) the first part corresponds to the time delay τ_J after J has jumped up, (ii) the next part corresponds to time, denoted by T_E^*, needed for the E-cell to reach RK_E^1 on $\mathcal{C}_1^R$ after jumping from $\mathcal{C}_0^R$ (corresponding to the part of the trajectory from P_2 to RK_E^1 in Fig. 3A), and (iii) after E jumps down, the third part, denoted by T_J^*, is the time needed for J to reach the right knee of $\mathcal{J}_0^R$ (corresponding to the trajectory from Q_2 to RK_J^0 in Fig. 3B). Combining all times yields $T_J^a = \tau_J + T_E^* + T_J^*$. Since the E-cell jumps up a delay τ_J after the J-cell jumps down, and the J-cell jumps up at the same time as the E-cell, the duration of the J-cell silent phase is $T_J^s = \tau_J$. Similarly, it can be seen that $T_E^a = \tau_J + T_E^*$ and $T_E^s = \tau_J + T_J^*$. Thus, the singular periodic solution exists if $T_J^{Lm} < \tau_J$ and $T_E^{Lm} < \tau_J + T_J^*$. In the latter inequality, the worst case occurs if the J-cell reaches RK_J^0 along $\mathcal{J}_1^R$ exactly when E jumps down, resulting in $T_J^* = 0$. Therefore, the singular periodic oscillatory solution populations exists if $\max(T_E^{Lm}, T_J^{Lm}) < \tau_J$.

Using similar arguments as above, we can compute T_E^a, T_E^s, T_J^a, the period $\mathcal{T}$ and the lower bound on τ_J for all other possible cases. These results are summarized in Table 2. Note that $T_J^s = \tau_J$ for all cases.

Now the lower bound on τ_J in condition (ii) of the theorem statement is the largest bound of those specified the last column of Table 2. Thus this lower bound on τ_J guarantees the existence of oscillatory solutions for both populations in all of the cases.

□

Stability. To proceed with stability analysis, we need to make some simplifying assumptions about the model. First, we assume the nonlinearity in the differential equation for the y coordinate in (2.4) and (2.6) can be written

$$g_E(x_E, y_E) = h_E(x_E) - k_E y_E, \qquad g_J(x_J, y_J) = h_J(x_J) - k_J y_J,$$

where $h_E,\ h_J$ are sigmoidal shaped nonlinearities. This is not a strong assumption, as this is the form of the differential equation for gating variables in many models. Second, we will assume the the sigmoids are steep enough that on the slow manifolds we have

$$h_E(\Phi_L^E(y_E, s_J)) \approx A_E^L,\ h_E(\Phi_R^E(y_E, s_J)) \approx A_E^R,$$

where $A_E^L > A_E^R$ are constants. Thus in the slow subsystem we have

$$y_E' = \left\{ \begin{array}{ll} k_E(A_E^L - y_E) & \text{when } x_E = \Phi_L^E(y_E, s_J(x_J(\tilde{t} - \tau_J)) \\ k_E(A_E^R - y_E) & \text{when } x_E = \Phi_R^E(y_E, s_J(x_J(\tilde{t} - \tau_J)). \end{array} \right\} \tag{3.1}$$

The equations for y_J follow analogously. The key effect of this assumption is that, on the slow manifolds, the y coordinate follows a linear differential equation which only depends on whether the cell is in the active or silent phase.

We can now state our main result.

Theorem 3.2. *Consider a network with one E-cell and one J-cell. Let the conditions of Theorem 3.1 be satisfied. If the cells are in cases $(1,k),(k,1),(2,3)$ of Table 2, the periodic solution is asymptotically stable. In the other cases it is stable if $T_E^s < T_E^a$ or $T_E^s > \frac{1}{k_E}\ln(2)$.*

Proof. To study the stability of the periodic orbits described above, we will construct a map similar to the approach in [34].

Consider an initial conditions as described in Theorem 3.1, with both cells on the right branch of the slow manifold, and the time history of both orbits in the silent phase, i.e., $(x_E(0),y_E(0)) = (x_{E0},y_{E0}) = P_0 \in \mathcal{C}_0^R$ and $(x_J(0),y_J(0)) = (x_{J0},y_{J0}) = Q_0 \in \mathcal{J}_1^R$. Assuming the initial conditions are close enough to the periodic orbit, the orbit corresponding to this initial condition should follow the right branches of the slow manifolds, jump to the left branches, follow them and then jump back up to the right branches. The simplified slow equations (3.1) can be integrated to get expressions for this orbit. Consider the E-cell and define $y_{Ed} = y_E(T_E^a)$ to be the y value at the jump down point (on the left branch) and $y_{Ef} = y_E(T_E^a + T_E^s)$ to be the y value at the jump up point, i.e. the final position on right branch. Then we have

$$\begin{aligned} y_{Ef} &= y_{Ed}e^{-k_E T_E^s} + A_E^L(1-e^{-k_E T_E^s}) \\ &= (y_{E0} - A_E^R)e^{-k_E(T_E^a+T_E^s)} + (A_E^R - A_E^L)e^{-k_E T_E^s} + A_E^L. \end{aligned}$$

The expression for the J-cell is completely analogous. Thus we can think of the trajectories of cells as a mapping from the $\mathcal{C}_0^R \times \mathcal{J}_1^R$ to itself. To simplify the mapping we introduce the shifted variables $u_E = y_{E0} - A_E^R,\ u_J = y_{J0} - A_J^R$. Then the mapping can be written

$$\begin{aligned} &H(u_E,u_J) \\ &= \left(u_E e^{-k_E(T_E^a+T_E^s)} + (A_E^L - A_E^R)(1-e^{-k_E T_E^s}), u_J e^{-k_J(T_J^a+T_J^s)} + (A_J^L - A_J^R)(1-e^{-k_J T_J^s})\right). \end{aligned}$$

The periodic solutions shown to exist in Theorem 3.1 correspond to fixed points $(\bar{u}_E,\bar{u}_J)$ of this map. The fixed points satisfy $T_E^a + T_E^s = T_J^a + T_J^s = \mathcal{T}$ and

$$\bar{u}_E = (A_E^L - A_E^R)\frac{1-e^{-k_E T_E^s}}{1-e^{-k_E \mathcal{T}}}, \quad \bar{u}_J = (A_J^L - A_J^R)\frac{1-e^{-k_J T_J^s}}{1-e^{-k_J \mathcal{T}}}. \tag{3.2}$$

To study the stability of the periodic solution we will consider the linearization of the map H about the fixed point $(\bar{u}_E,\bar{u}_J)$. While the map appears simple, as shown in Table 2, T_E^a, T_E^s, T_J^a depend on which trajectories the cells follow. In particular, these times may depend on the initial point of the trajectory through T_E^* etc. For example, consider an E-cell in Case 2. Since the cell jumps from the active to the silent phase when $y_E = y_E^R(1)$, we have $y_E^R(1) - A_E^R = u_E e^{-k_E(T_J+T_E^*)}$, which may be solved for T_E^*. Using a similar approach we have

$$\begin{aligned} T_E^* &= -\tau_J + \frac{1}{k_E}\ln\frac{u_E}{y_E^R(1)-A_E^R}, & T_E^\dagger &= \tau_J - \frac{1}{k_E}\ln\frac{u_E}{y_E^R(0)-A_E^R}, \\ T_J^* &= -T_E^a + \frac{1}{k_J}\ln\frac{u_J}{y_J^R(1)-A_J^R}, & T_J^\dagger &= T_E^a - \frac{1}{k_J}\ln\frac{u_J}{y_J^R(1)-A_J^R}. \end{aligned} \tag{3.3}$$

Using these expressions we can calculate the Jacobian matrix of the linearization, $DH_{i,j}$, for any case (i,j) of periodic orbit described in Table 2.

Straightforward calculations show the following

$$\begin{aligned} DH_{1,1}(\bar{u}_E,\bar{u}_J) &= \begin{pmatrix} e^{-k_E\mathcal{T}} & 0 \\ 0 & e^{-k_J\mathcal{T}} \end{pmatrix}; \\ DH_{1,j}(\bar{u}_E,\bar{u}_J) &= \begin{pmatrix} e^{-k_E\mathcal{T}} & \alpha\beta \\ 0 & 0 \end{pmatrix},\ j=2,3; \\ DH_{i,1}(\bar{u}_E,\bar{u}_J) &= \begin{pmatrix} 0 & 0 \\ -\frac{1}{\alpha}e^{-k_J\mathcal{T}} & e^{-k_J\mathcal{T}} \end{pmatrix},\ i=2,3. \end{aligned}$$

where $\alpha = \frac{k_E\bar{u}_E}{k_J\bar{u}_J}$ and

$$\beta = e^{-k_E\mathcal{T}}\left(\frac{A_E^L - A_E^R}{\bar{u}_E}e^{k_E T_E^a} - 1\right).$$

Clearly in these five cases, all the eigenvalues of the Jacobian matrix satisfy $|\lambda| < 1$, thus the periodic solutions are asymptotically stable.

Now consider the situation when both cells are in case 2. Then, using Table 2 and eq.(3.3) we have

$$\frac{dT_E^a}{du_E} = \frac{dT_E^*}{du_E} = \frac{1}{k_E u_E},\quad \frac{dT_E^s}{du_E} = \frac{dT_J^*}{du_E} = -\frac{1}{k_E u_E},\quad \frac{dT_E^s}{du_J} = \frac{dT_J^*}{du_J} = \frac{1}{k_J u_J}$$
$$\frac{dT_J^a}{du_E} = \frac{dT_E^*}{du_E} + \frac{dT_J^*}{du_E} = 0,\quad \frac{dT_J^a}{du_J} = \frac{dT_J^*}{du_J} = \frac{1}{k_J u_J}$$

It follows that

$$DH_{2,2}(\bar{u}_E,\bar{u}_J) = \begin{pmatrix} -\beta & \alpha\beta \\ 0 & 0 \end{pmatrix}$$

Similar calculations show that $DH_{2,3}, DH_{3,2}, DH_{3,3}$ are the same.

The eigenvalues in these latter cases are $0, -\beta$. Using eq. (3.2) we have

$$\beta = e^{-k_E T_E^s}\frac{1 - e^{-k_E T_E^a}}{1 - e^{-k_E T_E^s}}$$

If $T_E^s < T_E^a$ then

$$\frac{1 - e^{-k_E T_E^a}}{1 - e^{-k_E T u_E^s}} < 1,$$

while if $T_E^s > \frac{1}{k_E}\ln(2)$ then

$$\frac{e^{-k_E T_E^s}}{1 - e^{-k_E T_E^s}} < 1.$$

In either situation, $|\beta| < 1$. Noting from Table 2 that $T_E^s < T_E^a$ is always true in case $(2,3)$ concludes the proof. □

Remark 3.2. *The theorem above gives the stability for a network with multiple E-cells and J-cells assuming that each populations is synchronized, i.e., stability within the synchronization subspace. Stability to general perturbations could be considered using as similar approach but with higher dimensional maps. We leave this for future work.*

Corollary 3.1. *Let the conditions of Theorem 3.1 be satisfied with τ_J replaced by $\tau_E + \tau_J$. Then, a singular oscillatory periodic solution of the model (2.3)–(2.6) exists. If the conditions of Theorem 3.2 are also satisfied, with τ_J replaced by $\tau_E + \tau_J$, then the solution is asymptotically stable.*

Proof. The proof follows from the results of [39] which show that the important delays for determining the behaviour of a network are the total delays around any closed loop in the network. In our model (2.3)–(2.6) all the loops have the same total delay $\tau_{tot} = \tau_E + \tau_J$. Thus if the

model has a periodic solution with particular values of τ_E, τ_J such that $\tau_E + \tau_J = \tau_{tot}$ then the model has the same solution, with the same stability, for any values of τ_E, τ_J satisfying $\tau_E + \tau_J = \tau_{tot}$. All that will change is the relative phase difference of the E-cells and the J-cell. □

Remark 3.3. *The phase difference between the J-cell and the synchronized E-cells can be determined by the size of the excitatory synaptic delay, τ_E, regardless of the τ_J value. This is because the J-cell fires τ_E time after the E-cells fire. Specifically, if τ_E is set to be zero with nonzero τ_J, in-phase oscillations between J and E populations occur because the J-cell fires as soon as the E-cells fire. In contrast, if τ_E is nonzero, the J-cell fires τ_E time after the E-cells. Thus, oscillations between the two populations are out-of-phase with the phase lag, τ_E.*

(b) Dynamics with no delay

Using a similar approach to Section (a), we now show that a singular oscillatory solution, with the E-cells synchronized, does not exist if there is no time delay in the interaction between the two populations.

Theorem 3.3. *Suppose that there is no delay in the synapses for the globally inhibitory network, i.e., $\mathcal{T}_J = \mathcal{T}_E = 0$ in Eqs. (2.3)–(2.6), and that (i) in Theorem 3.1 is satisfied. Then a singular oscillatory periodic solution with the E-cells synchronized does not exist.*

Proof. In this situation, the slow subsystems of the E cells are as described by in (2.9)–(2.11) with $\tau_J = 0$ while the equations for the fast subsystem are obtained by setting $\epsilon = 0$ and $\mathcal{T}_J = \mathcal{T}_E = 0$ in (2.3)–(2.6).

We assume that the positions of E-cells are identical and show that no periodic solution exists as both the E-cells and J-cell always converge to their respective equilibrium points. There are several cases, depending on the initial conditions, i.e., the starting points of the two cell types, and the properties of nullclines. We analyze one case in detail, the others can be analyzed in a similar manner.

Suppose that both the E-cells and the J-cell start in the active phase, i.e., the E-cells lie on $\mathcal{C}_1^R$ and the J-cell on $\mathcal{J}_1^R$. As in the proof of Theorem 3.1, there are several cases for the solution trajectories depending on which cell type reaches the right knee of its respective nullcline first and the position this cell is in when the other cell type jumps down to the silent phase.

We consider one possible solution trajectory set as illustrated in Figure 6. As above, P_0 and Q_0 correspond to the starting points of the E and J cells, respectively. This figure corresponds to the case where the E-cells jump down first and the J-cell lies above RK_J^0 when E-cells jump down. In the figure, the cells evolve to points RK_E^1 and Q_1, respectively, then E-cells jump down to P_1 on $\mathcal{C}_1^L$. As this occurs, the J-cell jumps to $\mathcal{J}_0^R$, point Q_2. The J-cell follows the nullcline to RK_J^0, and then jumps down to its silent phase. In the case shown in Figure 6A, when this occurs the E-cell lies at point P_2 *above* LK_E^0. This makes it possible for the E-cells to jump up again as they are released from inhibition. Thus the E-cells jump to P_3 on $\mathcal{C}_0^R$ and the J-cell jumps to Q_3 on $\mathcal{J}_1^L$. The two cells then move along their respective nullclines until the E-cell reaches RK_E^0. The E-cells then jump down to $\mathcal{C}_0^L$, point P_4. This causes the J-cell to jump from $\mathcal{J}_1^L$ to $\mathcal{J}_0^L$, point Q_5. Since all cells are now in their silent phase with no synaptic input from the other cells, the convergence to the equilibrium points follows.

□

Remark 3.4. *This result holds for $\mathcal{T}_E$ and $\mathcal{T}_J$ sufficiently small. If $\mathcal{T}_E, \mathcal{T}_J$ are $O(\epsilon)$ then the delays will not appear in the equations for the fast and slow subsystems and the analysis will be the same as the zero delay case.*

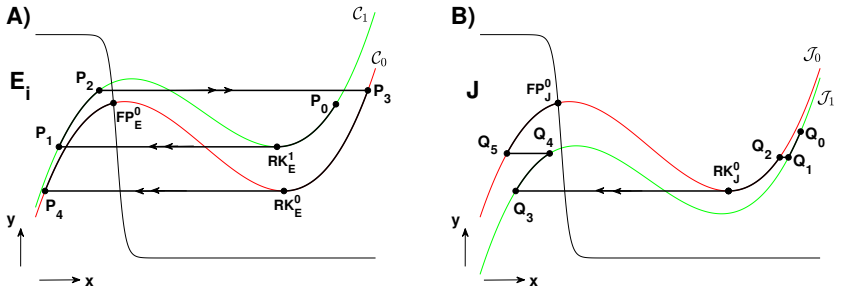

Figure 6. Plots of solution trajectories for A) E-cells and B) J-cell in black solid lines, approaching to their respective equilibrium points, if two populations start in the active phase and there is no delay in the synapses. These plots are for the case where E-cells lie above the left knee of the $s_J = 0$ cubic, corresponding to the red curve of A), when J jumps down.

4. Numerical Simulations

We conduct numerical simulations to illustrate the oscillatory solutions under different conditions on the nullclines for the E-cells and the J-cell, and on their delays, as constructed in Section 3. We consider a simple model by specifying explicit functions for f and g in Eqs. (2.3)–(2.4), for f_J and g_J in Eqs. (2.5)–(2.6), and synaptic variables s_i and s_J.

The model we consider is the following

$$\dot{x}_i = 3x_i - x_i^3 + y_i - g_{inh} s_J(x_J(t - \mathcal{T}_J))(x_i - x_{inh}), \tag{4.1}$$

$$\dot{y}_i = \epsilon(\lambda - \gamma \tanh(\beta(x_i - \delta)) - y_i), \tag{4.2}$$

$$\dot{x}_J = 3x_J - x_J^3 + y_J - g_{exc}\left(\frac{1}{N}\sum_i s_i(x_i(t - \mathcal{T}_E))\right)(x_J - x_{exc}), \tag{4.3}$$

$$\dot{y}_J = \epsilon(\lambda_J - \gamma_J \tanh(\beta_J(x_J - \delta)) - y_J), \tag{4.4}$$

where $i = 1, \ldots, 2$. Note that f and f_J are the same. Using different functions would not alter the results significantly. These functions are modified from those used in [8,64] so that the properties of f and g are as illustrated in Fig. 1. The function f is the same nonlinearity as in the FitzHugh-Nagumo [23,44] model, which is the simplest nonlinearity exhibiting a cubic x-nullcline. The function g is similar to the nonlinearity that occurs in equations for gating variables in conductance based models [22,49]. This parameters of this function allow us to easily adjust the behaviour of the model on the y-nullcline.

The parameters β, β_J denote the steepness of the sigmoidal curves for the y-nullcline and y_J-nullcline, respectively. We set both to be $\gg 1$. The parameters λ, γ, and δ for the E-cells are used to modify the amount of time they spend in the left or right branches as their speed along either branch depends on the y-nullcline. Model parameters for the J-cell, which are different from those for E-cells, are similarly defined.

The coupling function, s, is defined to be a sigmoid curve having the form of

$$s(x) = [1 + \exp(-(x - \theta)/\sigma)]^{-1}, \tag{4.5}$$

where σ determines the steepness of this sigmoid and is set to be $\ll 1$. The parameter θ is the threshold for x-variable, i.e., the value at which s rapidly changes from 0 to 1.

We used the delay differential equation solver in the numerical package XPPAUT [21] to numerically integrate Eqs. (4.1)–(4.4) with two E-cells and one J-cell and show the existence of

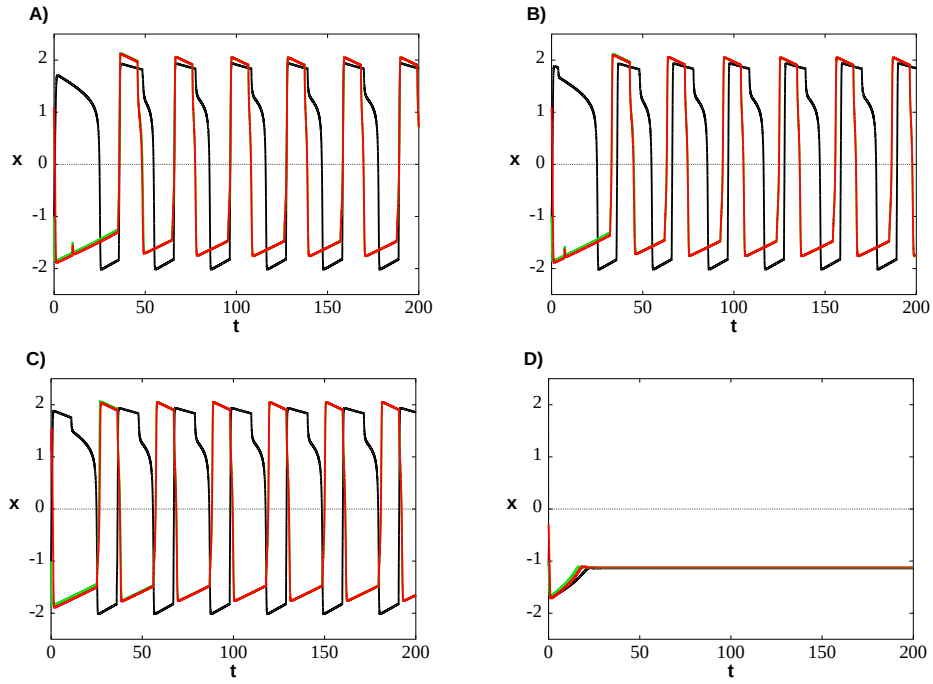

Figure 7. Example of case $(1,2)$ periodic solutions for two E-cells and one J-cell with different combinations of the two coupling delays. A) $\mathcal{T}_J = 10$ and $\mathcal{T}_E = 0$, B) $\mathcal{T}_J = 7$ and $\mathcal{T}_E = 3$, C) $\mathcal{T}_J = 0$ and $\mathcal{T}_E = 10$, D) $\mathcal{T}_J = 10$ and $\mathcal{T}_E = 0$. The black and red/green curves are the time courses of J-cell and E-cell voltages, respectively. Parameter values used are $\epsilon = 0.025,\ \gamma = \gamma_J = 5,\ \beta = \beta_J = 10,\ \delta = \delta_J = -1.1,\ \lambda = 1,\ \lambda_J = 0,\ \sigma = 0.002$, and $\theta = -0.5$. Coupling parameter values are $g_{exc} = g_{inh} = 1,\ x_{inh} = -3$, and $x_{exc} = 3$. For the simulations in A)–C) the initial conditions were given by eq.(4.6) with $x_{10} = -1, x_{20} = 1.1, y_{10} = 0.2, y_{20} = 0.02, x_{J0} = 1.1, y_{J0} = 0.1$. For D) they were the same except $x_{20} = -0.3, x_{J0} = -1.1$.

stable oscillatory solutions under the conditions of Theorem 3.1. We used constant initial functions

$$x_i(t) = x_{i0},\ y_i(t) = y_{i0},\ x_J(t) = x_{J0},\ y_J(t) = y_{J0},\ -\max\{\mathcal{T}_E, \mathcal{T}_J\} \le t \le 0, \tag{4.6}$$

where $i = 1, \ldots, 2$. The values for the constants are shown in the figure captions. Figure 7 shows an example of a case $(1,2)$ periodic orbit while Figure 8 shows an example of a case $(1,3)$ periodic orbit.

Note that the coordinates of the points $RK_E^0, RK_E^1, RK_J^0, RK_J^1$ can be found explicitly for the model (4.1)–(4.4). Using these and approximation (3.1) we estimated the times $T_E^R, T_E^{Rm}, T_J^R, T_J^{Rm}$ as per Table 1. Applying the lower bound in Table 2 for the parameter values of Figure 7 and converting the delays to the fast time gives the sufficient condition for oscillations $\mathcal{T}_J + \mathcal{T}_E > \max(T_E^{Lm} + T_E^L, T_J^{Lm})/\epsilon \approx 27.7$. In our simulations we observed oscillations for $\mathcal{T}_J + \mathcal{T}_E > 5.1$. For the parameter values of Figure 8 we obtained the condition $\mathcal{T}_J + \mathcal{T}_E > (T_E^{Lm} + T_E^L + T_J^{Lm} + T_J^L)/\epsilon \approx 54.7$. In our simulations we observed oscillations for $\mathcal{T}_J + \mathcal{T}_E > 37.6$. Clearly our estimates are conservative. This is not surprising since our analysis is based on the worst case analysis for the various cases of the trajectories.

Note that the periods and activation times are as predicted by Table 2 after converting these to the fast time. In both figures $T_E^a = \mathcal{T}_E + \mathcal{T}_J$, the total delay. In Figure 7 $T_J^a = \mathcal{T}_E + \mathcal{T}_J + T_J^* > T_E^a$ and the period is longer than $2(\mathcal{T}_E + \mathcal{T}_J)$ while in Figure 8 $T_J^a = \mathcal{T}_E + \mathcal{T}_J - T_J^\dagger < T_E^a$ and the period is shorter than $2(\mathcal{T}_E + \mathcal{T}_J)$. The period of the oscillation increases as the total delay is increased within the range where the stable oscillation exists. Although from Table 2 it would

appear the period depends linearly on the total delay, in fact the times $T_E^*, T_E^\dagger, T_J^*, T_J^\dagger$ can depend on the delay, so other than case $(1,1)$ the dependence is nonlinear.

In all simulations, the two E-cells (red and green curves) quickly synchronize on the periodic orbit. Further, as predicted by Corollary 3.1 identical periodic orbits with different phase difference between the E and J cells occur for different values of $\mathcal{T}_J$ and $\mathcal{T}_E$ with the same total delay. As noted in Remark 3.3, the phase difference between the two populations is determined simply by the size of the excitatory synaptic delay, $\mathcal{T}_E$. Part D) of each figure shows that an equilibrium point corresponding to the quiescent state coexists with the periodic orbit.

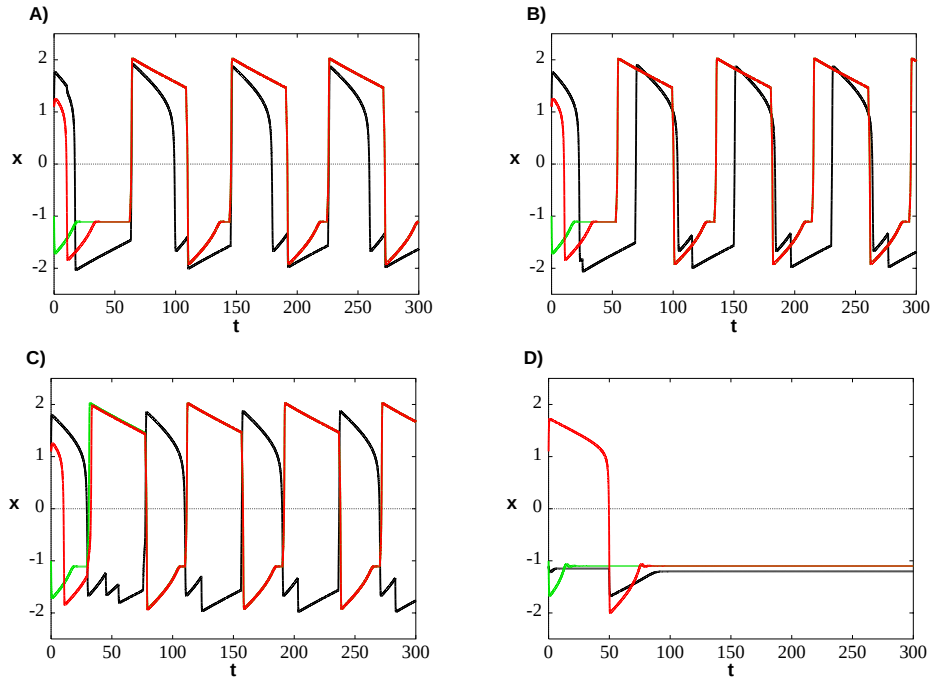

Figure 8. Example of case $(1,3)$ periodic solutions for two E-cells and one J-cell with different combinations of the two coupling delays. A) $\mathcal{T}_J = 45$ and $\mathcal{T}_E = 0$, B) $\mathcal{T}_J = 30$ and $\mathcal{T}_E = 15$, C) $\mathcal{T}_J = 0$ and $\mathcal{T}_E = 45$, D) $\mathcal{T}_J = 45$ and $\mathcal{T}_E = 0$. The black and red/green curves are the time courses of J-cell and E-cell voltages, respectively. Parameter values used are $\epsilon = 0.025,\ \gamma = \gamma_J = 5,\ \beta = \beta_J = 10,\ \delta = \delta_J = -1.1,\ \lambda = 2,\ \lambda_J = -2,\ \sigma = 0.002$, and $\theta = -0.5$. Coupling parameter values are $g_{exc} = g_{inh} = 0.5,\ x_{inh} = -2.2$, and $x_{exc} = 2.2$. In A)–C) the initial conditions were given by eq.(4.6) with $x_{10} = -1, x_{20} = 1.1, y_{10} = 0.2, y_{20} = 0.02, x_{J0} = 1.1, y_{J0} = 0.1$. For D) they were the same except $x_{J0} = -1.1$.

5. Discussion

In this paper, we provide sufficient conditions for the existence and stability of periodic solutions in which the excitatory cells are synchronized, in globally inhibitory networks of excitable cells with coupling delays. The model we develop and analyze is biologically motivated by several neural systems with this network structure. In the context of sleep rhythms, synchronization is one of the common rhythmic behaviors, in which excitatory thalamocortical relay cells fire together while receiving a global inhibition from a population of inhibitory thalamic reticular cells [18]. In sensory processing, synchronization through global inhibition can be important for a network of excitatory neurons to produce the correct response to a given input [19].

In Section 3, we apply geometric singular perturbation methods to prove existence and stability conditions in terms of the delays, $\mathcal{T}_J$ corresponding to the delay in inhibitory synapses and $\mathcal{T}_E$ corresponding to that in excitatory synapses. These delays represent both the time for information to travel between neurons and to be processed at the synapse. We show that the presence of delays makes it possible for the network to exhibit synchronous periodic solutions. In contrast, if there is no delay in both synapses, our analysis demonstrates that synchronous periodic solutions cannot be obtained. Based on the construction of synchronous periodic solutions under certain conditions, we determined the period of such solutions in terms of the lengths of both delays.

In related studies by Rubin and Terman [49,51], they assume that the inhibitory cells have a longer active phase than the excitatory cells, based on the experimental findings that thalamic reticular cells are known to have longer active states than relay cells [18]. However, as we indicate above, global inhibitory networks occur in other neural systems, where this assumption may or may not be true. Thus, we extend their analysis by giving conditions that do not depend on the length of the active phase of either cell type, and show synchronous solutions can exist as long as there are sufficiently long delays. In particular, applying the results of [39], we show that the size of the total delay $\mathcal{T}_E + \mathcal{T}_J$ is the important parameter for synchronous periodic solutions to exist, with the specific sizes of $\mathcal{T}_E$ and $\mathcal{T}_J$ determining the relative phase of spiking in the excitatory and inhibitory populations.

We provide numerical simulations using XPPAUT [21] in Section 4 to supplement and validate the analytical results in Section 3. We specify explicit forms for the nonlinearities in our generic two-dimensional, relaxation oscillator model, Eqs. (2.3)–(2.6), which have appropriate form for the nullclines. The numerical simulations of this model confirm that the presence of the delay in at least one synapse type is an essential factor to generate oscillations with the E-cells synchronized.

One advantage of the explicit representation of coupling delays in model equations, is that we can conduct a systematic study for the existence of solutions depending on the length of delays. This allows us to extend the way that the effect of synaptic delays were incorporated in previous models of global inhibition [49,51] while having slightly simpler model equations. Thus, in Section 4, we consider three different combinations of inhibitory and excitatory delays for each case of which cell has the longer active phase. The model simulations demonstrate that all of the combinations result in synchronized behaviors among the excitatory cells. These synchronized oscillations differ from each other only in terms of the phase difference between excitatory and inhibitory cells' oscillations; their qualitative features are the same.

In addition, our model extends the work on the effect of delays in [8,24] in that ours analyzes a network of excitable neurons with both excitatory and inhibitory synapses whereas theirs focused on system with excitatory neurons which are oscillatory, that is, where each uncoupled neuron can oscillate without synaptic coupling.

Our model extends some of previous modeling work on synaptic delays in biologically relevant neural networks. However, analysis on other types of network behaviors, such as clustered patterns, is also needed to obtain a more complete understanding of how different population rhythms arise as a result of the interaction between coupling delays, intrinsic properties of each cell and network architecture. Also, since the present model assumes that J population is nearly synchronized so that it can be viewed as a single cell, we can relax this condition by allowing the interaction between neurons in the J population, which may result in different population behaviors other than synchronization, such as clustering. Investigating the role of the interactions between inhibitory thalamic reticular cells in the thalamocortical networks is worthy of further investigation in the context of network firing patterns.

Funding. The first author was supported by a University of Hartford Greenberg Junior Faculty Grant. This support does not necessarily imply endorsement by the University of Hartford of project conclusions. The second author was supported by a grant from the Natural Sciences and Engineering Research Council of Canada.

References

1. Barton, D., Krauskopf, B., Wilson, R.: Periodic solutions and their bifurcations in a non-smooth second-order delay differential equation.
   Dyn. Sys. **21**(3), 289–311 (2006)
2. Beierlein, M., Gibson, J., Connors, B.: A network of electrically coupled interneurons drives synchronized inhibition in neocortex.
   Nat. Neurosci. **3**(9), 904–910 (2000)
3. Bezaire, M., Soltesz, I.: Quantitative assessment of CA1 local circuits: knowledge base for interneuron-pyramidal cell connectivity.
   Hippocampus **23**(9), 751–785 (2013)
4. Bose, A., Manor, Y., Nadim, F.: Bistable oscillations arising from synaptic depression.
   SIAM J. Appl. Math. **62**(2), 706–727 (2001)
5. Burić, N., Todorović, D.: Dynamics of Fitzhugh-Nagumo excitable systems with delayed coupling.
   Phys. Rev. E **67**, 066–222 (2003)
6. Buzsáki, G., Llinás, R., Singer, W., Berthoz, A., Chrtisten, Y. (eds.): Temporal coding in the brain.
   Springer–Verlag, New York, NY (1994)
7. Campbell, S., Wang, Z.: Phase models and clustering in networks of oscillators with delayed coupling.
   Physica D **363**, 44–55 (2018)
8. Campbell, S.R., Wang, D.: Relaxation oscillators with time delay coupling.
   Physica D **111**(1), 151–178 (1998)
9. Chandrasekaran, L., Matveev, V., Bose, A.: Multistability of clustered states in a globally inhibitory network.
   Physica D **238**(3), 253–263 (2009)
10. Choe, C.U., Dahms, T., Hövel, P., Schöll, E.: Controlling synchrony by delay coupling in networks: From in-phase to splay and cluster states.
    Phys. Rev. E **81**(2), 025205 (2010)
11. Chow, S.N., Lin, X.B., Mallet-Paret, J.: Transition layers for singularly perturbed delay differential equations with monotone nonlinearities.
    J. Dyn. Differ. Equ. **1**(1), 3–43 (1989)
12. Connors, B., Long, M.: Electrical synapses in the mammalian brain.
    Annu. Rev. Neurosci. **27**, 393–418 (2004)
13. Contreras, D., Destexhe, A., Sejnowski, T., Steriade, M.: Spatiotemporal patterns of spindle oscillations in cortex and thalamus.
    J. Neurosci. **17**(3), 1179–1196 (1997)
14. Crook, S., Ermentrout, G., Vanier, M., Bower, J.: The role of axonal delay in synchronization of networks of coupled cortical oscillators.
    J. Comput. Neurosci. **4**, 161–172 (1997)
15. Dahms, T., Lehnert, J., Schöll, E.: Cluster and group synchronization in delay-coupled networks.
    Phys. Rev. E **86**(1), 016202 (2012)
16. Destexhe, A., Bal, T., McCormick, D.A., Sejnowski, T.J.: Ionic mechanisms underlying synchronized oscillations and propagating waves in a model of ferret thalamic slices.
    J. Neurophysiol. **76**, 2049–2070 (1996)
17. Destexhe, A., Mainen, Z., Sejnowski, T.: Kinetic models of synaptic transmission.
    In: C. Koch, I. Segev (eds.) Methods in Neuronal Modeling: From Synapses to Networks, chap. 1. MIT Press, Cambridge, MA (1998)
18. Destexhe, A., Sejnowski, T.J.: Synchronized oscillations in thalamic networks: Insights from modeling studies.
    In: M. Steriade, E.G. Jones, D.A. McCormick (eds.) Thalamus. Elsevier, Amsterdam (1997)
19. Doiron, B., Chacron, M., Maler, L., Longtin, A., Bastian, J.: Inhibitory feedback required for network oscillatory responses to communication but not prey stimuli.
    Nature **421**(6922), 539–543 (2003)
20. Douglas, R., Martin, K.: Recurrent neuronal circuits in the neocortex.
    Curr. Biol. **17**(13), R496–R500 (2007)
21. Ermentrout, E.: Simulating, analyzing, and animating dynamical systems: a guide to XPPAUT

for researchers and students, vol. 14.
SIAM (2002)
22. Ermentrout, G., Terman, D.: Mathematical Foundations of Neuroscience.
Springer, New York, NY (2010)
23. Fitzhugh, R.: Impulses and physiological states in theoretical models of nerve membrane.
Biophysical J. **1**, 445–466 (1961)
24. Fox, J.J., Jayaprakash, C., Wang, D., Campbell, S.R.: Synchronization in relaxation oscillator networks with conduction delays.
Neural Comput. **13**(5), 1003–1021 (2001)
25. Fridman, E.: Effects of small delays on stability of singularly perturbed systems.
Automatica **38**(5), 897–902 (2002)
26. Fukuda, T., Kosaka, T.: Gap junctions linking the dendritic network of gabaergic interneurons in the hippocampus.
J. Neurosci. **20**(4), 1519–1528 (2000)
27. Golomb, D., Rinzel, J.: Clustering in globally coupled inhibitory neurons.
Physica D **72**, 259–282 (1994)
28. Golomb, D., Wang, X.J., Rinzel, J.: Synchronization properties of spindle oscillations in a thalamic reticular nucleus model.
J. Neurophysiol. **72**(3), 1109–1126 (1994)
29. Golomb, D., Wang, X.J., Rinzel, J.: Propagation of spindle waves in a thalamic slice model.
J. Neurophysiol. **75**(2), 750–769 (1996)
30. Jacklet, J. (ed.): Neuronal and cellular oscillators.
Marcel Dekker Inc, New York, NY (1989)
31. Kim, S., Park, S.H., Ryu, C.: Multistability in coupled oscillator systems with time delay.
Phys. Rev. Lett. **79**, 2911–2914 (1997)
32. Kim, U., Bal, T., McCormick, D.: Spindle waves are propagating synchronized oscillations in the ferret LGNd in vitro.
J. Neurophysiol. **74**(3), 1301–1323 (1995)
33. Kopell, N., LeMasson, G.: Rhythmogenesis, amplitude modulation, and multiplexing in a cortical architecture.
Proc. Natl. Acad. Sci. USA **91**(22), 10,586–10,590 (1994)
34. Kunec, S., Bose, A.: Role of synaptic delay in organizing the behavior of networks of self-inhibiting neurons.
Phys. Rev. E. **63**(2), 021908 (2001)
35. Kunec, S., Bose, A.: High-frequency, depressing inhibition facilitates synchronization in globally inhibitory networks.
Network: Comput. Neural Sys. **14**(4), 647–672 (2003)
36. Landisman, C., Long, M., Beierlein, M., Deans, M., Paul, D., Connors, B.: Electrical synapses in the thalamic reticular nucleus.
J. Neurosci. **22**(3), 1002–1009 (2002)
37. Llinás, R.R.: The intrinsic electrophysiological properties of mammalian neurons: insights into central nervous system function.
Science **242**(4886), 1654–1664 (1988)
38. LoFaro, T., Kopell, N.: Timing regulation in a network reduced from voltage-gated equations to a one-dimensional map.
J. Math. Biol. **38**(6), 479–533 (1999)
39. Lücken, L., Pade, J., Knauer, K.: Classification of coupled dynamical systems with multiple delays: Finding the minimal number of delays.
SIAM J. Appl. Dyn. Syst. **14**(1), 286–304 (2015)
40. Luzyanina, T.: Synchronization in an oscillator neural network model with time-delayed coupling.
Network: Comput. Neural Sys. **6**, 43–59 (1995)
41. Mallet-Paret, J., Nussbaum, R.: Global continuation and asymptotic behaviour for periodic solutions of a differential-delay equation.
Ann. Mat. Pura Appl. **145**(1), 33–128 (1986)
42. Miller, J., Ryu, H., Teymuroglu, Z., Wang, X., Booth, V., Campbell, S.A.: Clustering in inhibitory neural networks with nearest neighbor coupling.
In: T. Jackson, A. Radunskaya (eds.) Applications of Dynamical Systems in Biology and Medicine, pp. 99–121. Springer, New York (2015)

43. Mishchenko, E.F., Rozov, N.K.: Differential equations with small parameters and relaxation oscillations, vol. 13.
Springer, New York, NY (1980)
44. Nagumo, J., Arimoto, S., Yoshizawa, S.: An active pulse transmission line simulating nerve axon.
Proceeding IRE **50**, 2061–2070 (1962)
45. Orosz, G.: Decomposition of nonlinear delayed networks around cluster states with applications to neurodynamics.
SIAM J. Appl. Dyn. Syst. **13**(4), 1353–1386 (2014)
46. Poo, C., Isaacson, J.: Odor representations in olfactory cortex: “sparse" coding, global inhibition, and oscillations.
Neuron **62**(6), 850–861 (2009)
47. Rinzel, J., Terman, D., Wang, X.J., Ermentrout, B.: Propagating activity patterns in large-scale inhibitory neuronal networks.
Science **279**(5355), 1351–1355 (1998)
48. Roux, L., Buzsáki, G.: Tasks for inhibitory interneurons in intact brain circuits.
Neuropharmacology **88**, 10–23 (2015)
49. Rubin, J.E., Terman, D.: Analysis of clustered firing patterns in synaptically coupled networks of oscillators.
J. Math. Biol. **41**, 513–545 (2000)
50. Rubin, J.E., Terman, D.: Geometric analysis of population rhythms in synaptically coupled neuronal networks.
Neural Comput. **12**(3), 597–645 (2000)
51. Rubin, J.E., Terman, D.: Geometric singular perturbation analysis of neuronal dynamics.
Handbook of Dynamical Systems **2**, 93–146 (2002)
52. Sethia, G., Sen A.and Atay, F.: Phase-locked solutions and their stability in the presence of propagation delays.
Pramana **77**(5), 905–915 (2011)
53. Sieber, J.: Dynamics of delayed relay systems.
Nonlinearity **19**(11), 2489–2527 (2006)
54. Sieber, J., Kowalczyk, P., Hogan, S., Di Bernardo, M.: Dynamics of symmetric dynamical systems with delayed switching.
J. Vib. Control **16**(7-8), 1111–1140 (2010)
55. Skinner, F., Kopell, N., Marder, E.: Mechanisms for oscillation and frequency control in reciprocally inhibitory model neural networks.
J. Comput. Neurosci. **1**, 69–87 (1994)
56. Somers, D., Kopell, N.: Rapid synchronization through fast threshold modulation.
Biol. Cybern. **68**(5), 393–407 (1993)
57. Steriade, M., Jones, E.G., Llinás, R.R.: Thalamic oscillations and signaling.
Wiley, New York, NY (1990)
58. Sun, X., Li, G.: Fast regular firings induced by intra- and inter-time delays in two clustered neuronal networks.
Chaos **28**, 106310 (2017)
59. Sun, X., Li, G.: Synchronization transitions induced by partial time delay in a excitatory–inhibitory coupled neuronal network.
Nonlinear Dyn. **89**, 2509–2520 (2017)
60. Sun, X.M., Zhao, J., Hill, D.: Stability and L_2-gain analysis for switched delay systems: A delay-dependent method.
Automatica **42**(10), 1769–1774 (2006)
61. Terman, D., Ermentrout, G., Yew, A.: Propagating activity patterns in thalamic neuronal networks.
SIAM J. Appl. Math. **61**(5), 1578–1604 (2001)
62. Terman, D., Kopell, N., Bose, A.: Dynamics of two mutually coupled inhibitory neurons.
Physica D **117**, 241–275 (1998)
63. Terman, D., Lee, E.: Partial synchronization in a network of neural oscillators.
SIAM J. Appl. Math. **57**, 252–293 (1997)
64. Terman, D., Wang, D.: Global competition and local cooperation in a network of neural oscillators.
Physica D **81**(1), 148–176 (1995)

65. Tomasi, S., Caminiti, R., Innocenti, G.: Areal differences in diameter and length of corticofugal projections.
Cereb. Cortex **22**(6), 1463–1472 (2012)
66. Traub, R.D., Miles, R.: Neuronal networks of the hippocampus.
Cambridge University Press, New York, NY (1991)